electronic reprint

Journal of
Applied Crystallography
ISSN 0021-8898
Editor: **Anke R. Kaysser-Pyzalla**

Direct observation of *B*-site cation displacements in Pb-based complex perovskite relaxor oxides

K. Z. Baba-Kishi

J. Appl. Cryst. (2011). **44**, 111–121

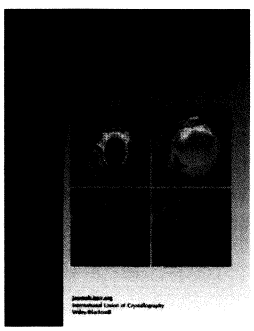

Journal of
Applied Crystallography
ISSN 0021-8898

Received 18 March 2010
Accepted 18 October 2010

Direct observation of *B*-site cation displacements in Pb-based complex perovskite relaxor oxides

K. Z. Baba-Kishi

Department of Applied Physics, The Hong Kong Polytechnic University, Kowloon, Hong Kong. Correspondence e-mail: apakzbab@polyu.edu.hk

Electron diffraction patterns recorded using a scanning transmission electron microscope (STEM) from $PbMg_{1/3}Nb_{2/3}O_3$ (PMN) crystallites and $PbZn_{1/3}Nb_{2/3}O_3$ (PZN) crystals show weak and systematic continuous diffuse streaking along the ⟨110⟩ directions. Detailed high-angle annular dark-field (HAADF) images recorded *via* an aberration-corrected STEM show that the *B*-site cations in PMN and PZN undergo correlated and long-range displacements towards the Pb^{2+} ions on the (110) planes. The planar *B*-site displacement measured from the centres of the octahedra is about 0.3–0.5 Å in PMN and about 0.20–0.4 Å in PZN. In the HAADF images of the PMN crystallites and PZN crystals studied, there is insufficient evidence for systematic long-range planar displacements of the Pb^{2+} ions. The observed Pb^{2+} ion displacements in PMN and PZN appear randomly distributed, mostly displaced along ⟨110⟩ towards the *B*-site columns. There is also evidence of possible stress-related distortion in certain unit cells of PMN. In the relaxors studied, two distinct types of displacements were observed: one is the long-range planar *B*-site spatial displacement on the (110) planes, correlated with the Pb^{2+} ions, possibly resulting in the observed diffuse streaking; the other is short-range Pb^{2+} ion displacement on the (110) planes. The observed displacement status indicates a mutual attraction between the Pb ions and the *B*-site cations in which the *B* sites undergo the largest spatial displacements towards the Pb ions along ⟨110⟩.

1. Introduction

Pb-based relaxor oxides are important functional materials that exhibit an intriguing array of local and crystal structures, which vary depending on whether the crystal is in the paraelectric (PE), ferroelectric (FE), antiferroelectric or frustrated incommensurate antiferroelectric state (Baba-Kishi & Pasciak, 2010). In the case of $PbSc_{1/2}Ta_{1/2}O_3$ (PST), for example, a well known relaxor, the transition from the PE to the FE state entails a space-group change from *Pm*3*m* or *Fm*3*m* to *R*3*m* or *R*3, respectively (Woodward & Baba-Kishi, 2002). Most relaxors, including $PbMg_{1/3}Nb_{2/3}O_3$ (PMN) and PST, have a tendency to undergo structural evolution and may be viewed as adaptable structures (Withers *et al.*, 1994). The structural evolution could include chemical long-range order of various degrees associated with a superstructure on the (111) planes and development of an additional superstructure associated with long-range clustering of *B*-site cations on the (100) planes in PST (Baba-Kishi *et al.*, 2006). In addition, *A*-site and *B*-site displacements occur as a combined result of lone-pair electrons on Pb^{2+} and the necessity of meeting the valence requirements by the Pb^{2+} ions, *e.g.* in $PbSc_{1/2}Nb_{1/2}O_3$ (Knight & Baba-Kishi, 1995) and $PbZn_{1/3}Nb_{2/3}O_3$ (PZN; Welberry *et al.*, 2006). In PST, the progression from the PE to the FE state has been determined to entail Pb ion displacements in at least three different directions in the FE state, whereas in the PE state, the average Pb^{2+} displacements appear to be aligned primarily along the ⟨110⟩ directions (Woodward & Baba-Kishi, 2002).

In the Pb-based complex perovskite-structured relaxors, the *A* site is occupied by the Pb atom and the *B* sites may be occupied by two species of cations, namely *B*′ and *B*″. The 1:1 or 2:1 ideal columnar occupational stoichiometric ratio depends on whether the composition is 1:1, *e.g.* as in PST, or 2:1 as in $PbMg_{1/3}Nb_{2/3}O_3$ or $PbZn_{1/3}Nb_{2/3}O_3$. There is evidence suggesting that the larger of the *B*-site cations, *B*′, is ferroelectrically inactive and that the Pb ion is attracted to the larger cation (Chen *et al.*, 1996). These authors propose that the smaller cation, *B*″, is ferroelectrically active and wanders about within the octahedron, free from Pb—O—*B*″ couplings. Chen *et al.* (1996) place emphasis on size preference in Pb—O—B bonding that leads to cation alloying, which they propose to elucidate the relaxor behaviour. Strong coupling that takes place between the Pb ions and the ferroelectrically active smaller *B*-site cations through oxygen bonding leads to a random environment. These findings are supported by the studies carried out by Davies & Akbas (2000), suggesting that well ordered cation occupancies conflict with the notion of a 'space-charge' model and favour the 'random-site' model for the *B*-site long-range order. Long-range chemical clustering of

B-site cations under certain conditions has been proposed to result in a specific superstructure in PST (Baba-Kishi *et al.*, 2006). Positional displacements of the Pb ions on the *A* site are favoured by chemical ordering between Sc^{3+} and Nb^{5+} in $PbSc_{1/2}Nb_{1/2}O_3$, as reported by Perrin *et al.* (2001).

Extensive studies carried out by Welberry *et al.* (2005, 2006), Welberry & Goossens (2008) and Pasciak *et al.* (2007), using atom-based Monte Carlo models, have shown that nanoscale polar domains occur in PZN (Fig. 1*a*) and other relaxors, resulting in diffuse streaking observed along the ⟨110⟩ directions [simulated in Fig. 1(*b*)]. Individual domains thus simulated are thin plate-like domains oriented normal to the ⟨110⟩ directions, consequently resulting in diffuse streaks along ⟨110⟩, as observed in their X-ray diffraction patterns. The Monte Carlo simulations require nanoscale domains that are formed by the necessity of the Pb ions to attain their necessary valence states, thus forcing the Pb^{2+} ions to displace away from the centres of their 12-fold coordination polyhedra with an in-plane displacement towards one of the coordination O atoms (Fig. 1*c*). In these studies, the proposition for the *B*-site cations, Zn and Nb, in PZN is to alternate in the ⟨100⟩ directions, but their complete long-range order is frustrated by the 2:1 stoichiometry, presumably suggesting that, in the 1:1 stoichiometry (as in PST), the distribution of Sc^{3+} and Ta^{5+} is ordered in equal proportions. It is further pointed out that no diffraction evidence has been found to show that the *B*-site cation ordering is directly linked to the proposed nanoscale polar domains (which originate from Pb displacements), and, if such a linkage occurs, the effects must be subtle. The directionality in Pb^{2+} displacement is inferred to arise from the stereochemical lone-pair electrons on Pb^{2+}.

In the models proposed by Welberry & Goossens (2008) and Pasciak *et al.* (2007), domains or domains wall boundaries, respectively, oriented along [110] cooperatively generate the observed diffuse streaks. It is proposed in these studies that such a scenario of cooperative Pb displacements, as the fundamental generators of diffuse streaking, occurs or should occur in all the Pb-based relaxors. These authors have calculated that the magnitude of the Pb ion displacement is about 0.50 Å. According to Welberry & Goossens (2008), bond-valence calculations show that the Pb^{2+} ions attain their correct valence in a regular coordination polyhedron by displacing directly towards one of the oxygen ions. The lone pair, which gives directionality to the Pb displacement, is directed diametrically opposite to ⟨110⟩ and towards the most distant O atom. However, studies carried out by Dmowski *et al.* (2000) show that the Pb ions are displaced along the ⟨100⟩ directions in the context of the local and average structures.

The purpose of this article is to present the results of high-angle annular dark-field (HAADF) studies performed on PMN ceramics and PZN crystals using a chromatic aberration-corrected (Cs-corrected) scanning transmission electron microscope (STEM). The HAADF–STEM observations are compared with the findings reported in the atom-based Monte Carlo simulation studies. The study of PMN and PZN by the Cs-corrected HAADF technique is an attempt at an assessment of consistency in the observations made in the relaxor ceramics and crystals, both of which have 2:1 stoichiometry regimes in the observed structures.

2. Experimental

The specimens of PMN and PZN were crushed in a solution of ethanol immediately preceding electron microscopy; the use of crushed samples eliminated key uncertainties in image interpretation attributed to sample preparation by ion milling, including ion-beam-induced damage and ion implantation. Crushing the specimens also ensured that the sample surfaces were atomically clean by being free from oxidation. The electron microscopes used were the JEOL JEM 2011 (TEM), JEM 2010F (Cs-corrected STEM) and JEM-ARM200F (Cs-corrected STEM). The specimens of PZN, grown from high-

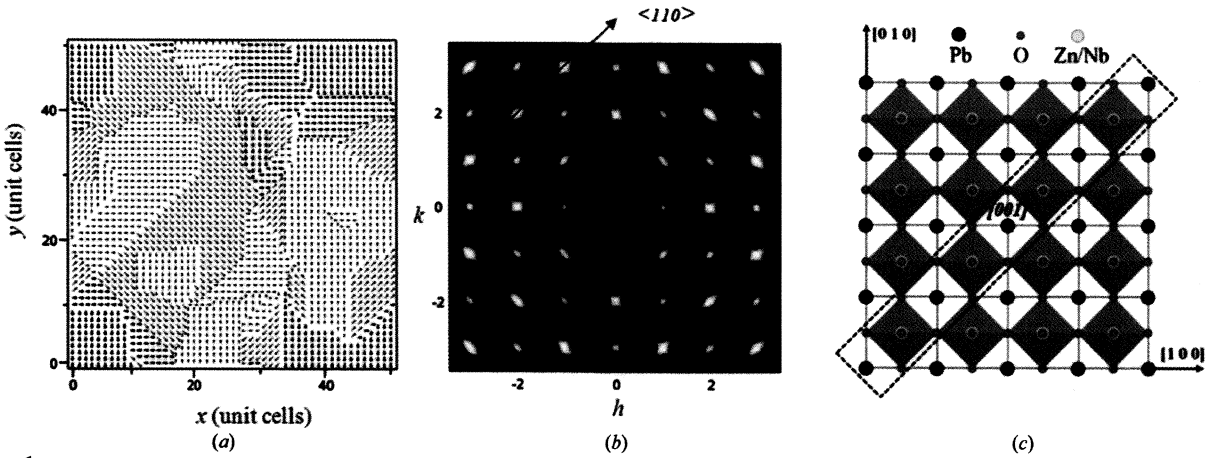

(*a*) (*b*) (*c*)

Figure 1
Polar nano-domains and their boundaries, simulated *via* Monte Carlo methods (*a*), result in streaking along the ⟨110⟩ directions, observed in the simulated diffraction pattern (*b*) projected along [001] (Pasciak *et al.*, 2007). (*c*) Schematic diagram showing the projection of the PZN structure along [001] and the fault plane position along [110] on the (110) planes with Pb as the origin of the unit cell. (*a*)/(*b*) and (*c*) were provided by M. Pasciak and D. J. Goossens, respectively.

temperature solution (Zhang *et al.*, 2000), were supplied by Richard Welberry for this study. The PMN ceramics were prepared by the standard mixed-oxide route. The software used to carry out line plots, measurements on the images and Fourier transforms was *Digital Micrograph* (Gatan Inc., Pleasanton, CA, USA).

Measurements were carried out on the HAADF images from PMN and PZN following image calibration. The known interatomic distance of 4.07 Å between the two Pb atomic columns along ⟨100⟩ was used to calibrate the images for several times and in various locations on the image. The atomic columns along ⟨110⟩ were not used for calibration owing to the presence of displacements of both the Pb and the *B*-site columns. For calibration, the image had to be magnified so as to display the smallest possible visible pixel, as shown in Fig. 2. The measuring tool of the software was able to measure to the nearest pixel, which represented its maximum resolution capability. The cursor placed on the image for measurement always automatically spanned the length of one single pixel, as the smallest element on the image. In calibrating the images, two intrinsic problems were encountered: the first problem was that each pixel in the image represented a maximum attainable resolution of about 0.17 Å and could not therefore be improved; the second was that the intensity blob in pixels representing an atomic column was rarely circular and centred, thus causing an error of at least 0.17 Å in locating the atomic column centres. Consequently, a deviation from the centre of the column by one pixel entailed an error of at least 0.17 Å. The measurements performed on the images of PMN often carried an error such than the measured displacements of the *B*-site positions varied in the range 0.30–0.70 Å; the smallest displacement measured was about 0.27 Å. Most commonly, the measured displacements were approximately 0.50 Å in PMN. In PZN, the measured displacements of the *B*-site columns were in the range 0.20–0.40 Å, including the minimum error of 0.17 Å.

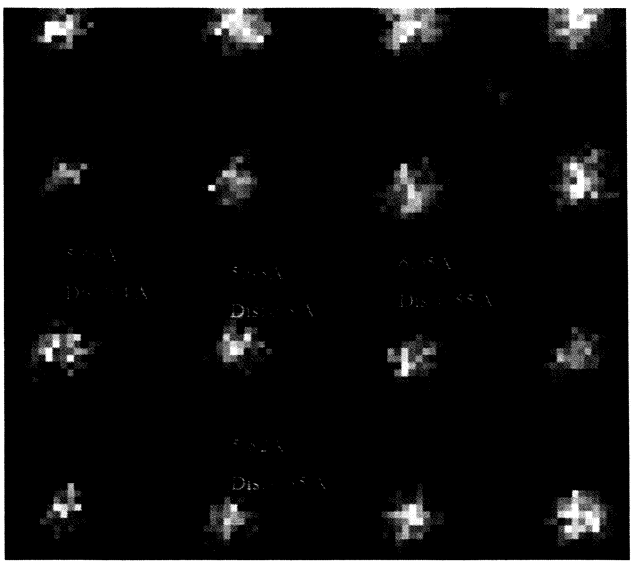

Figure 2
To calibrate an image for measuring displacements, the image was magnified to display the smallest measurable pixilation. Each pixel in this HAADF image is about 0.17 Å across. Error occurred through lack of precision in identifying the centres of the atomic columns. The largest number displayed in each box is the measured separation between the two Pb atomic columns (two highest intensities) along ⟨110⟩; the measured displacement (Dis) of the *B*-site column from the nearest Pb column is also shown in each box.

3. Observations

In this article, the morphological characteristics of the observed planar *B*-site displacements in PMN and PZN, investigated *via* a Cs-corrected STEM and observed in the HAADF images, are presented. The HAADF images are interpreted qualitatively by Fourier transforms and by extensive measurements. The geometrical characteristics of the diffracted diffuse streaks recorded from PMN and PZN using a TEM are discussed first.

3.1. The characteristics of diffuse streaking as observed in the electron diffraction patterns from PMN and PZN

A variety of relaxor ceramics and crystals studied, including PMN ceramics and PZN crystals, exhibit continuous diffuse streaking along the ⟨110⟩ directions. To illustrate, electron diffraction patterns recorded along the [001] directions in PMN and PZN are shown in Figs. 3(*a*) and 3(*b*), respectively. Notable features of the streaks are that they pass through all the diffracted spots along the ⟨110⟩ directions, are very weak in intensity, display moderate broadening and exhibit different intensities in each of the diffraction patterns. The observed intensities of the streaks are relative to the background in each pattern and may not be considered as true intensities owing to the influence of dynamical scattering in thick specimens, as well as the prevailing recording and exposure conditions of the diffraction patterns. The patterns are indexed using the space group *Pm*3*m* with lattice parameter 4.07 Å, but they may also be indexed using the *Fm*3*m* space group with lattice parameter 8.14 Å, depending on whether the preference is for the disordered structure or the chemically long-range-ordered superstructure, respectively (Baba-Kishi *et al.*, 1992; Woodward & Baba-Kishi, 2002; Baba-Kishi & Pasciak, 2010). The morphology of the streaks observed in the diffraction patterns of these relaxors obtained using the STEM is independent of the crystal tilt, but their intensities may naturally enhance or weaken depending on the scattering conditions used in the TEM, as well as on the orientation of the specimen. In relaxors, the influence of position on intensities is important because it is related to differences in the chemical composition between two different positions. If the positions are adjacent, the influence of specimen thickness can be ignored. Owing to the facts that the streaks are weak and that the dynamical scattering is strong in the selected-area diffraction patterns, any streak passing through the centre of the diffraction pattern becomes invisible or very difficult to observe and record, even when the specimen is tilted.

Diffuse scattering is relatively weak and concentrated around the direct beam. However, given that the intensity in the direct beam is being shared strongly with numerous other diffracted beams that are close together in reciprocal space, there will be a contribution of diffuse scattering from each diffracted beam, resulting in smearing out of the weak diffuse scattering around the centre of the diffraction pattern. However, as we move away from the centre, the strong dynamical scattering eases, allowing the weak streaks to become visible. Careful inspection of the patterns shows that very weak streaks are present at the centres of the diffraction patterns, although they are very difficult to reproduce here. As we will note in the study of the HAADF patterns, any systematic long-range displacive *B*-site disorder should entail the presence of the streaks at the centre of the diffraction pattern. It is thought unlikely therefore that transverse polarized scattering is present in these patterns. An account of the nature of transverse polarized scattering in $Pb(ZrTi)O_3$ is given by Baba-Kishi *et al.* (2008).

Another important consideration in the behaviour of the streaks is the influence of temperature. Knowledge of the temperature dependency of the streaks is crucial in understanding whether the various transition states have any influence on the occurrence of the streaks. *In-situ* cooling and heating experiments carried out with the TEM on various crystals and ceramics of PST have revealed that the streaks remain in the diffraction patterns (not shown in this article), regardless of the temperature applied to the crystal. The temperatures at which the streaks were observed in PST were in the range 400–180 K. Studies carried out by Mihailova *et al.* (2008) indicate that there is a relationship between the streak behaviour at low temperature and the FE transition. Although this observation may be associated with the degree of long-range order of the specific specimen used, it has not been possible to observe this phase transition in the TEM patterns at 180 K. In the case of the TEM patterns from PST (Fig. 4), any enhancement of the streak intensity may be attributed, at least partially, to a reduction in thermal diffuse scattering. It may thus be difficult to distinguish any intensity changes that originate from a phase transition. Detailed discussion of the temperature dependency of the streaks and their association with phase transition falls beyond the scope of this article, but may be found in the article by Mihailova *et al.* (2008). A fundamental conclusion reached by cooling the specimens of PST in the TEM is that the streaks had retained their presence, morphology, broadness and orientations along the ⟨110⟩ directions. Assuming that a certain disorder leads to the streaks in the PE state (400 K), it was then deduced from these results that the same disorder is present in the FE state (180 K). Consequently, the streaks were ubiquitous to both the PE and the FE states in PST. For illustration, a diffraction pattern recorded from PST at 180 K along [001] is shown in Fig. 4, clearly demonstrating the orientation of the streaks, which are also commonly observed in ceramics of PST and PMN. The orientations of the streaks match those of the

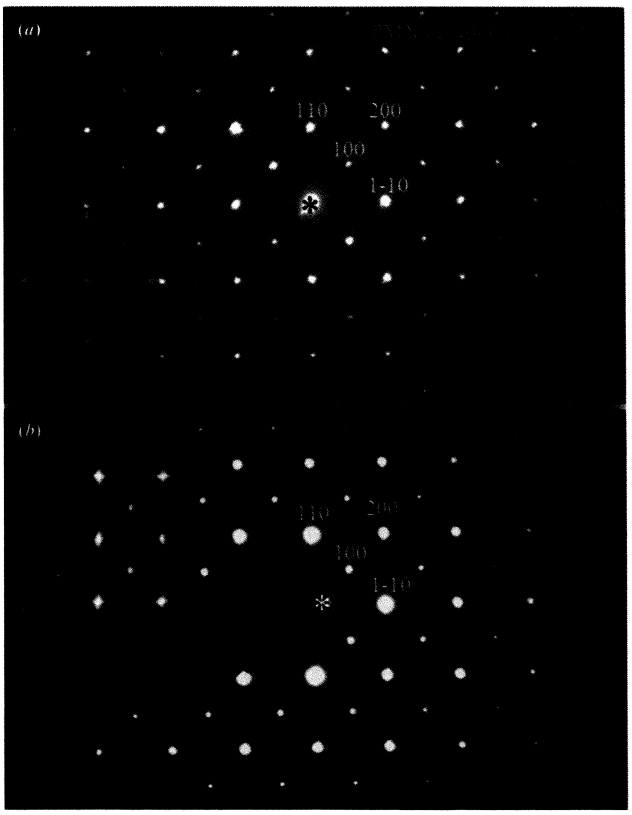

Figure 3
Electron diffraction patterns recorded along [001] from (*a*) the PMN ceramic crystallite and (*b*) the PZN single crystal. The diffraction patterns exhibit very weak diffuse streaking along ⟨110⟩, marked in (*a*). Large open arrows on the patterns show extremely weak streaks that pass through the centres of the patterns – the scattering is unlikely to be transverse polarized. Inset of (*b*): the streaks in the diffraction pattern from PZN can be compared with its simulated Monte Carlo pattern (Fig. 1*b*).

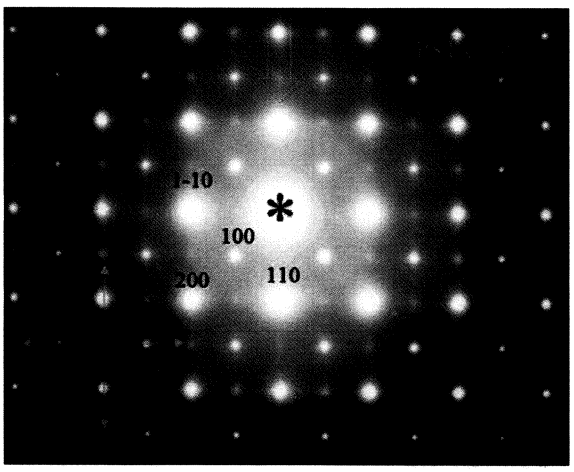

Figure 4
The symmetry of the diffuse streaks can be seen in the diffraction pattern recorded at 180 K from a PST crystal. At this temperature the crystal is in the FE state. The streaks have been recorded at various other temperatures including the PE state temperature (240 K). Two mutually perpendicular ⟨110⟩-oriented diffuse streaks, shown with cyan arrows, are visible passing through the centre of the diffraction pattern.

streaks simulated by the Monte Carlo method, shown in Fig. 1(*b*).

3.2. Cs-corrected scanning transmission electron microscopy of PMN and PZN

Atomic resolution HAADF is an average atomic number sensitive technique (*Z*-contrast technique), allowing differential intensities arising from dissimilar atomic species to be observed. In HAADF, incoherent thermal scattering dominates the image intensity, while contributions from Bragg diffraction are minimized. The incoherent thermal scattering in a STEM is much less sensitive to changes in defocus and specimen thickness than the high-resolution imaging in a TEM. The atomic columns in an HAADF image appear as white features, making direct qualitative interpretation of the image relatively simple. In this study, the HAADF–STEM images are interpreted qualitatively in order to determine the geometry of the ion displacements. Quantitative investigation of the intensities associated with columnar occupancies is beyond the scope of the present study. For the various characteristics of HAADF scanning transmission electron microscopy, the reader is referred to Pennycook & Jesson (1990, 1991), James & Browning (1999), Krivanek et al. (2003), Klenov et al. (2007) and Molina et al. (2007).

3.2.1. Observed *B*-site cation displacements in PMN. In a search for direct observation of any ion displacement, extensive electron microscopy studies were carried out using a Cs-corrected STEM. Fig. 5 is a Cs-corrected HAADF–STEM image recorded from a crushed sample of a PMN crystallite, the image being representative of several images recorded from different crystallites of PMN. The image originates from a thin area of the sample, whose thickness was estimated to be less than 500 Å. The sample had a clean surface, made possible by transferring the particle of the crushed sample into the STEM immediately after crushing. There is therefore no possibility of oxidation on the surface. The fact that the sample was not prepared for the STEM by ion milling removes the possibility of substantial uncertainties in interpreting the image.

In Fig. 5, the columns of the Pb atoms are the largest and brightest features in the image. The separation between the two nearest Pb atomic columns along the [010] or [100] direction is 4.07 Å (nominal lattice parameter of PMN when referred to *Pm*3*m*). The nominal separation between the two nearest Pb atomic columns in the unit cell along the [110] direction is 5.760 Å. The Pb atoms along [110] are sandwiched by columns of the *B*-site cations, whose ideal positions are at the centre of the oxygen octahedron (thus exactly midway between the two Pb columns) and whose columnar occupancy along the column is supposed to ideally follow the stoichiometry defined by Mg (1/3):Nb (2/3).

The *B*-site cations must be located symmetrically at the centre of the unit cell, precisely half way (about 2.89 Å) between the two Pb columns of 5.760 Å separation according to the established structure. Significantly, the image in Fig. 5 shows that the *B*-site ions are displaced towards one of the Pb atoms along [110] and away from the opposite Pb atom along [1$\bar{1}$0]. We can also clearly see across the whole image that the *B*-site cations have undergone substantial cooperative displacements in correlation with the columns of the Pb ions. To visualize the displacements in Fig. 5, a row of *B*-site cations are joined together by a diagonal solid red line, while the adjacent rows of Pb ions are joined by two cyan lines, illustrating that the *B*-site cations are not equidistant from the their adjacent Pb ions. To further illustrate the displacements, a row of Pb ions and *B*-site cations are joined together by short solid blue lines, showing that the Pb and *B*-site atoms are not positioned along a straight vertical line but instead alternate (zigzag) along [110] with respect to each other. The measured planar *B*-site cation displacement with respect to the Pb planes is approximately 0.50 (20) Å. To show the systematic and long-range morphology of the *B*-site cation displacements with respect to the Pb ions, an unaltered original HAADF image is

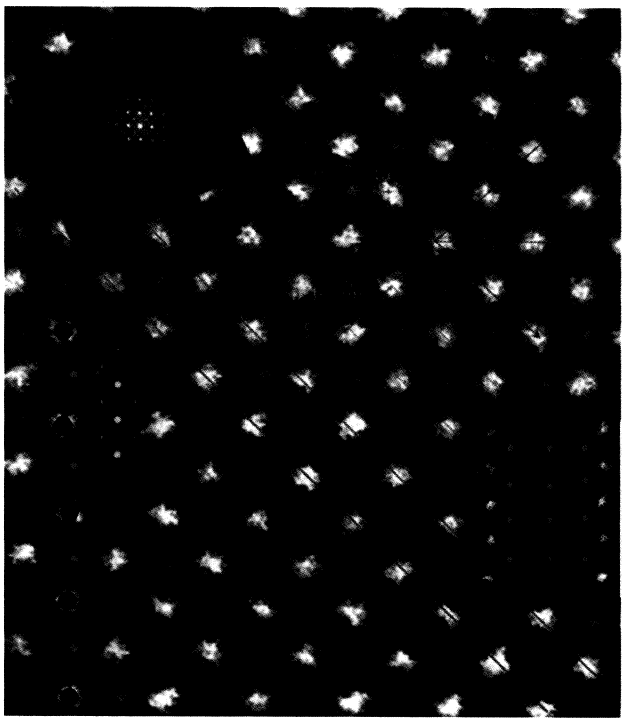

Figure 5
HAADF image recorded from a PMN crystallite along [001], illustrating the displacements of the *B*-sites cations correlated with the Pb ions. The magnitude of these displacements is approximately 0.50 (20) Å directed along ⟨110⟩. The off-centring of the *B*-site cations can be seen in the lower rectangular blue box – the inset above this blue box shows the streaking perpendicular to the direction of the cation displacement. The inset at the top left of the image shows the large-area diffraction pattern oriented to match the orientation with the HAADF image. The figure is marked variously to show the crystallographic directions and the lattice constants. The separation between the two Pb columns along [001] is about 4.07 Å (*Pm*3*m*). The separation between the two Pb columns along [110] is 5.76 Å. Lines drawn diagonally on the image show the unequal separation between rows of Pb ions and a row of the *B*-site cations. In the lower-right inset, solid yellow circles are roughly superimposed on *B*-site positions in the actual image, showing the relative *B*-site displacements (yellow circles) with respect to the Pb ions (red circles).

presented in Fig. 6(*a*). The pattern shows that all the *B*-site cations are displaced over a long range in the structure with respect to the Pb ions. Fig. 5 is an enlarged section of Fig. 6(*a*) selected for analysis.

To illustrate the *B*-site cation displacements, various HAADF images recorded from PMN were analysed by the standard methods of fast Fourier transform (FFT), inverse fast Fourier transform (IFFT), pseudo-contouring and line plots. The image in Fig. 6(*a*) was processed using the 'reduced' mode of the FFT and IFFT analyses, which allows the FFT to be performed on the entire image. It is assumed that the specimen thickness was 500 Å. The resulting IFFT image in Fig. 6(*b*) is almost identical to the original image in Fig. 6(*a*). The spots selected for producing the IFFT image included the various outer spots in the FFT diffraction pattern (inset of Fig. 6*b*). There is, therefore, agreement between the real image and the IFFT results, confirming that *B*-site displacements are indeed present in PMN.

To further substantiate the *B*-site displacements, a series of three IFFT images are shown in Figs. 7(*a*)–7(*c*). Each image is analysed slightly differently by placing dissimilar masks over the available diffracted spots produced in the FFT patterns, which are shown in the insets of their respective images. The IFFT image in Fig. 7(*a*) clearly shows the *B*-site cations displaced with respect to the Pb ions, as observed in the HAADF image in Fig. 5. To generate this IFFT image, the outer spots in the FFT pattern were included. By not including the outer spots in the IFFT calculations, the *B*-site displacements were less easy to reproduce in the IFFT images, as shown in Fig. 7(*b*) and its FFT inset. The *B*-site displacements are also reproduced in Fig. 7(*c*), which included the various outer spots and their surrounding diffuse intensities. A simple explanation for the influential role of the outer spots in producing *B*-site displacements in the IFFT images is that, under conditions of strong systematic diffraction along a zone axis, the dynamical diffraction causes sharing of scattering between all the strongly diffracted electron beams. Away from the centre, the dynamical scattering is weaker, allowing the streaks to become visible. By including the outer spots and their surrounding diffuse intensities, we include those weakly scattered beams that originate from the structural displacements. It is recognized that the sharp vertical and horizontal streaks observed in the FFT patterns are artefacts originating from the edge effects and other anomalies in the FFT process and are therefore unrelated to the weak continuous streaks that arise from structural displacements. The component of the streaks that originates from the real displacements could not be readily observed by eye in the FFT patterns. The image in Fig. 7(*d*) is an informative image reproduced by 'pseudo-contouring' the IFFT image in Fig. 7(*c*). This image clearly shows the 'dumbbell' effect generated by the proximity of the displaced *B* sites relative to the Pb ions. The image is qualitative but serves to show clear visual evidence of the *B*-site displacements in PMN.

The overall *B*-site displacement morphology is illustrated by line plots produced by placing a line on a row of atom images that includes Pb only along [010], *B*-site cations only along [010], and a combination of Pb and *B* sites only along [110]. The line plots, which are essentially the records of atomic column intensities with reference to the background, were performed on well calibrated HAADF patterns or their IFFT counterparts. The line plots in Fig. 8(*a*) represent the intensities vertically and the atom-separation distances horizontally recorded from a row of Pb atoms. The measured interatomic spacings of the Pb ions correspond to approximately 4.0 Å. The plot clearly shows that the Pb ions are equidistant along [010]. Similarly, the line plot in Fig. 8(*b*), recorded from a row of *B* sites adjacent to the Pb ions along

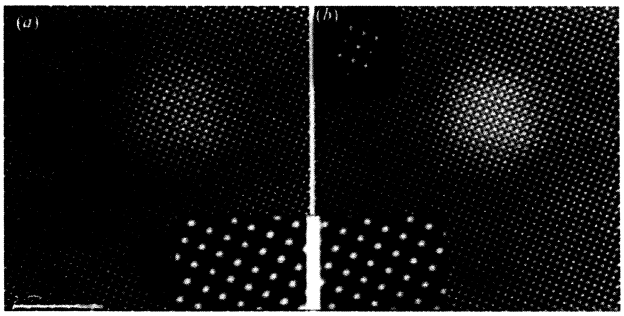

Figure 6
(*a*) HAADF image showing systematic long-range displacements on the *B* sites with respect to the Pb ions. (*b*) 'Reduced' IFFT recorded from (*a*) – almost identical to the original image. The spots selected are illustrated in the inset of (*b*). To retain the original configurations, the figures are not enlarged or altered. Enlarged details of the images are shown in their insets. The scale bar is 5 nm.

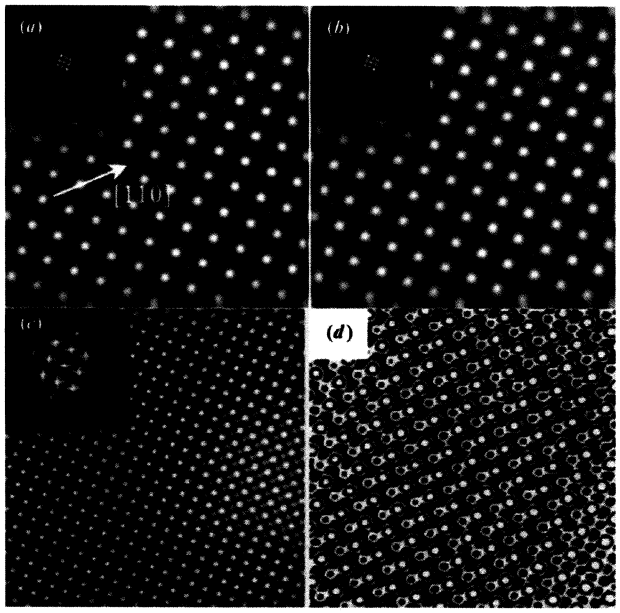

Figure 7
(*a*)–(*c*) FFT and IFFT performed on a section from Fig. 6(*a*), clearly illustrating the displacement of the *B*-site cations along [110] in correlation with the Pb ions, except in (*b*) which was processed by excluding the outer spots in the FFT pattern [see the inset in (*b*)]. (*d*) A pseudo-contour image produced from (*c*), showing the *B*-site displacements as a 'dumbbell' feature in the image.

[010], shows a measured interatomic separation of 4.0 Å, close to the spacing in PMN (see also Fig. 5). The *B*-site cations are also equidistant from one another. However, a line plot (Fig. 8*c*) recorded from a row of Pb ions and *B*-site cations together along the [110] direction shows unequivocally that the *B*-site cations are displaced (off-centred) towards the Pb ions along [110], while the Pb ions are in their nominal 4.0 Å positions, undisplaced.

In order to measure the relative displacements of the *B* sites differently, surface plots recorded from the Pb ions along [010], *B*-site cations along [010], and Pb ions and *B*-site cations along [110] were used, as in Fig. 9, where all the interatomic distances are marked. The surface plots show that both the Pb ions and the *B*-site cations have identical interatomic separations along [010] and that they are undisplaced relative to each other, whereas the *B* sites along [110] are displaced by about 0.50 Å relative to the Pb ions, which remain undisplaced. An important observation here is that the Pb ions appear fixed in their nominal positions; they are therefore nominally symmetrical about the unit-cell origin, apart from some sporadic stress-related Pb displacements in certain localities discussed later in the text. Careful inspection also shows that there is intensity sharing between the Pb and *B* sites (inclined towards the *B* sites) along [110], indicating that the displacements of the Pb ions and the *B* sites are mutual, with an implication that the Pb ions are also displaced by certain distances from their mean positions. However, Pb displacements are not readily resolved in the HAADF images or in the surface plots.

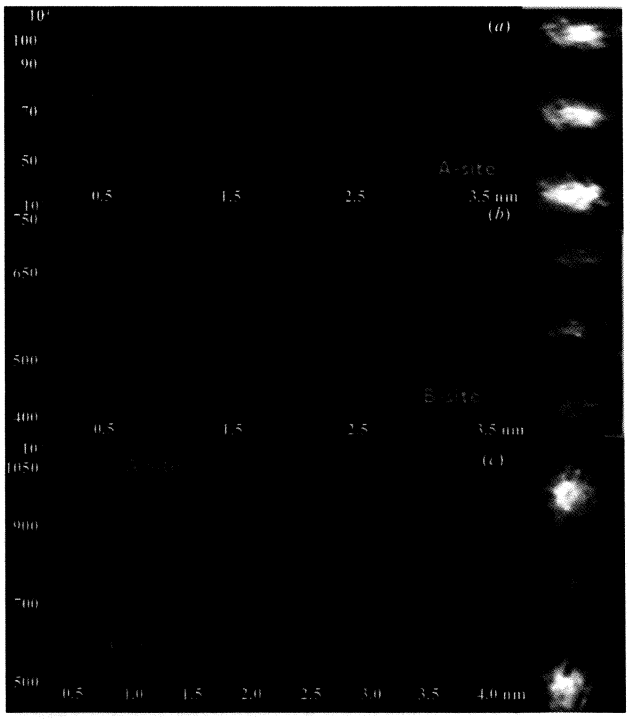

Figure 8
Intensity *versus* distance line plots in PMN, shown for (*a*) Pb ions only along [010], (*b*) *B*-site cations only along [010], and (*c*) Pb and *B* sites combined along [110]. The displacement of the *B*-site cations towards the Pb sites can clearly be seen in (*c*). Vertical insets: strips of HAADF images from PMN (Fig. 5) showing the correspondence between the line plots and the atomic rows.

3.2.2. Pb displacements in PMN. In addition to the surface and line plots, another way to observe the atomic displacements on the HAADF images is by superimposing a calibrated square of pre-determined dimensions onto the unit cell such that the edges of the square coincide with the centres of the atoms on the image as best as visually possible. This square is then repeatedly stacked side by side on the unit cells ensuring as little an error as possible. Either the Pb or the *B* site was selected as the origin, as illustrated in Figs. 10(*a*) and 10(*b*). In Fig. 10(*a*), the Pb ions are selected as the origin of the unit cell. The red square was affixed onto the unit cell as the calibrated unit cell. The blue squares, which are identical to the calibrated unit cell, were then stacked side by side following the red square. In Fig. 10(*b*), the Pb ions appear located mostly at the centres of their unit cells, while the *B* sites (yellow dots) are displaced towards the Pb ions, as the delineations indicate.

In this image, however, it appears that some of the Pb ions are deviated away from their centres towards the *B* sites along ⟨110⟩, indicating a mutual displacement between the Pb ions and the *B*-site cations, as we have noted in the surface plots of Fig. 9. Importantly, not all the Pb ions are cooperatively displaced along ⟨110⟩; some appear shifted towards the inside of the unit cell, possibly as a result of stress in the structure, whereas some others are shifted towards the *B* sites. A few of these Pb ions are marked with open arrows for illustration. The overall shift observed in the positions of the Pb ions relative to the original unit cell indicates an apparent compression or perhaps a rotation in the imaged structure. At the same time, the *B*-site cations marked with solid yellow circles in Fig. 10(*a*) show consistent and correlated displacements along ⟨110⟩. By choosing the *B* sites as the unit-cell origin, as in Fig. 10(*b*), we note that the Pb ions exhibit no

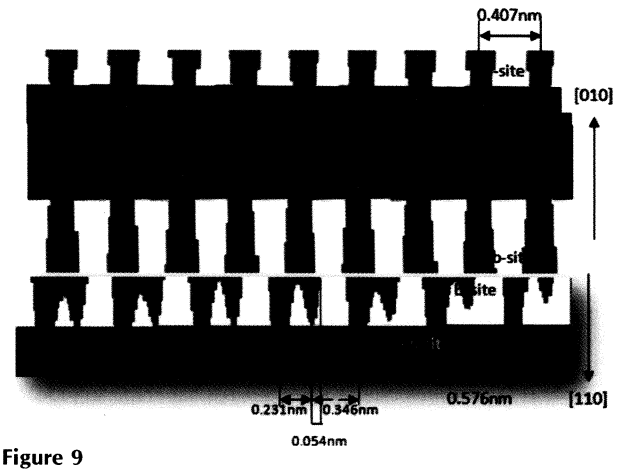

Figure 9
Intensity *versus* distance surface plots for Pb and *B* sites only along [010], and Pb and *B* sites combined along [110], showing unambiguously that the *B* sites are displaced toward the Pb ions by a measured distance of about 0.50 Å in PMN. All the other ions, according to these plots, are apparently unperturbed. The measured interatomic distances, the atomic species and their directions are marked on the diagram.

observable long-range displacements relative to the *B* sites. However, the unit cell containing the four *B* sites is displaced towards the unit cell containing the four Pb ions.

On superimposing the calibrated squares onto the HAADF images, a small rotation in the Pb-containing unit cell is indicated; this rotation appears to be directed anticlockwise, towards the displaced *B* sites along [110], as illustrated in Fig. 10(*d*). We note in this image that the unit cell is distorted in the anticlockwise direction. However, the use of this method to substantiate the Pb displacements or their rotation is rather erroneous, because of several factors including the error in calibrating a unit cell and in identifying the centres of the atoms, which exhibit asymmetrical intensities surrounding the centres of the atomic columns. We have measured the *B*-site displacements as 0.50 (20) Å in PMN, but it has not been possible to quantify any correlated Pb displacements that might be present in the structure with certainty. By visual examination, however, and by using many images processed by IFFT transforms, we note a mutual attraction between the Pb and the B sites along [110]. Inspecting the spatial closeness or intensity coupling between the Pb and B sites in Fig. 10(c), it appears plausible that the Pb ions are shifted towards the B sites by some distance, perhaps by about 0.20 Å.

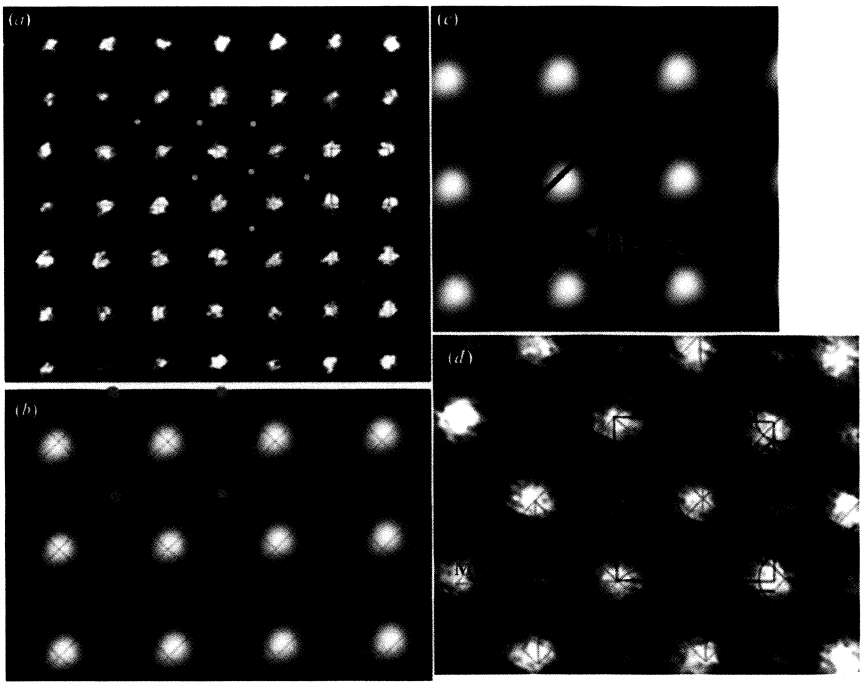

Figure 10
Images recorded along [001] from PMN. (*a*) The Pb ion is selected as the origin of the unit cell, where the *B*-site cations show systematic long-range displacements (solid yellow circles) along ⟨110⟩. Some of the Pb ions are also displaced, mostly towards the *B* sites, but appear uncorrelated over the long range. The Pb ions shown with open arrows seem to have displacements towards the inside of the unit cell, a possible cause of distortion in the structure. (*b*) The *B* site (solid yellow circles) is selected as the origin of the unit cell in the FFT image extracted from (*a*). Certain Pb ions are off-centre (an example is shown with the cyan open arrow). (*c*) IFFT image, showing intensity coupling between the Pb and *B* sites, a likely indication of a mutual shift between the Pb and *B* sites. (*d*) The displacement of the Mg/Nb cations along ⟨110⟩ towards the Pb site (red circle). The red square indicates an apparent rotational distortion in the Pb unit cell.

This method of analysis might entail the question as to how the *B* sites displace rather than the Pb sites and not *vice versa*. Selecting the Pb site as the origin, it has been possible to connect all of the *B*-site sublattices together with square grids, which form a regularly displaced lattice structure correlated over an extended and long-range space, uninterrupted. The long-range nature of the *B*-site perturbations with respect to the well formed regular (110) planes defines a fault plane that is likely to result in diffuse streaking, which is the indicator of directionality in the displacements. On the other hand, the Pb^{2+} displacements, with Pb selected as the origin of the unit cell, are irregular and uncorrelated over the long range. This irregularity could well be responsible for the high displacement parameters observed in the neutron diffraction (Woodward & Baba-Kishi, 2002), indicating the presence of displacements on the Pb sites, but the magnitude of these displacements might be too small or too uncorrelated to be quantified in the present STEM images.

3.2.3. PZN. Cs-corrected HAADF–STEM images recorded from crushed samples of PZN have also revealed long-range *B*-site cation displacements towards the Pb ions along the ⟨110⟩ directions, analogous to the displacements observed in PMN crystallites. An example of the images from PZN is shown in Fig. 11. In this image, the unit cells, with each cell centred on a Pb ion, are placed in squares to aid with visualization. In each square, the *B*-site cation must be located at the centre of the unit cell, which is also the centre of the oxygen octahedron. Measurements and qualitative analysis of the image show that the *B*-site cations are displaced towards the Pb ions in a correlated fashion. The red circles placed at the centres of the squares on the image show the expected positions of the *B*-site cations.

The apparent displacements of the *B*-site cations in PZN are not as large as those observed in PMN. The difference between the displacements in PZN and PMN is estimated to be about 0.20 Å. This large difference could only be explained (albeit with conjecture) by concluding that the displacement regimes in these relaxors are influenced by the fundamental properties of the *B*-site species, such as their atomic radii and charges. Columnar *B*-site non-stoichiometry is also likely to influence correlated planar displacements. This value was measured using various spatial line profiles recorded along the [110] rows of atoms that contain both the Pb and the *B* sites, but it is considered as an approximate value. The methodology

used to measure the displacements in PMN revealed a lowest measured value of about 0.3 Å and a highest measured value of 0.7 Å.

A representative example of a line profile is illustrated in Fig. 11(*b*), showing a measured displacement of about 0.25 Å in PZN. The lines are not equidistant because the *B*-site cations are displaced cooperatively on the (110) planes towards the Pb ions, effectively creating planar faults analogous to PMN. No evidence of systematic Pb ion displacements could be found in PZN, partly perhaps because of the resolution limits of the images recorded. Evidence collected by the use of repeated surface and line plots on the images supports displacement variability in the *B*-site cation positions along different columns. This could well arise from errors in the measurements as discussed in §2. Since it is not possible to carry out a precise quantitative numerical analysis of these displacements, the displacement variability of the *B* sites can only be subject to conjecture. Distortions in Pb positions towards the *B* sites are visually apparent in the images but are difficult to quantify.

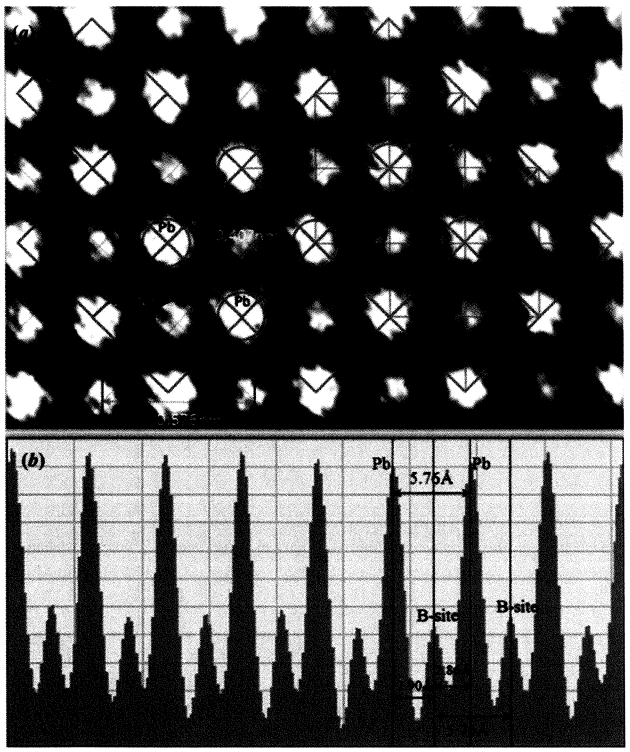

Figure 11
HAADF image recorded along [001] from PZN showing the contrast differences between the Pb ions (brightest) and those of the Zn/Nb cations on the *B* site (less bright). Cyan squares delineate the octahedra projected onto the flat plane. The displacement of the *B*-site cations with respect to the Pb ions can be seen by visualizing that each *B* site must be located precisely at the centre of its octahedron. The yellow lines show the unequal distances. The *B*-site cations displaced with respect to the red circles (marking the centre of the unit cell) exhibit dissimilar intensities within a close proximity to each other. The average difference in intensities is likely to arise from clustering of different species of cations along the columns. Beam illumination and specimen thickness within the imaged area are constant. Observable displacements could not be seen on the Pb ions. O atoms are invisible.

4. Discussion

Extensive STEM–HAADF studies show unambiguously that the *B*-site cations undergo measurable displacements along the ⟨110⟩ directions in PMN and PZN. It appears that the cooperative characteristics of the *B*-site cation displacements could adequately explain the presence of the continuous diffuse streaking in the diffraction patterns, at least in terms of the directionality of the streaks. According to the HADDF images, the displacement originates from the planar (110)-type interfaces perpendicular to [110] in correlation with the Pb planes. The primary condition for generating diffuse streaking is to include two-dimensional additional correlations in the structure. These correlations can involve planar domains (Welberry & Goossens, 2008) or planar domain boundaries (Pasciak *et al.*, 2007). There is also the condition that a component of the atomic displacement is correlated within a certain plane. The *B*-site cations are displaced along the ⟨110⟩ directions in correlation with the planes of the Pb ions on the (110)-type interface, satisfying the conditions for the presence of the streaks in the patterns. Based on the observations, the mutual attraction between the Pb ions and *B*-site cations along [110] also satisfies this condition of the presence of the (110)-type interface.

Long-range planar Pb^{2+} displacements could not be observed in PMN and PZT, but sporadic localized Pb^{2+} displacements along ⟨110⟩ and ⟨100⟩ were observed in PMN. There are indications in many of the HAADF images, especially in the PMN images, that small Pb displacements exist in the unit cells, particularly directed along [110] towards the *B* sites. According to the HAADF results, not every Pb ion undergoes displacement. The objective is not to state that Pb displacements do not exist but to state that *B*-site cations undergo substantial long-range displacements in the structures studied. We note that the *B*-site species clearly have a profound influence on the Pb displacement regimes in PMN and PZN. The *B*-site columns may have differing stoichiometries that influence the way the Pb ions function, including the influence on their displacement magnitudes.

The long-range *B*-site planar displacements observed in the HAADF images tend to reduce the need to construct numerous individual nano-domains or nano-domain walls to generate the streaks. The planar nature of the *B*-site displacements explains the origin of the streaking observed. The Pb displacements along [110] are also likely to contribute partially to the streaks. In the case of the projected [001] direction, there is essentially a set of four domains only; each domain is oriented in one of the four ⟨110⟩ directions and each direction is perpendicular to one of the (110) planes. This arrangement leads to a set of four mutually perpendicular streaks, as observed in the diffraction patterns arising from the *B*-site and possibly the *A*-site displacements. According to the observations reported here, it seems unlikely that the Pb^{2+} ions are solely responsible for the streaks, though they also

undergo displacements along [110]. HAADF images from PMN adequately illustrate that the Pb and *B*-site ions are mutually attracted in the ⟨110⟩ direction. The measured displacement of 0.50 (20) Å in PMN, when combined with the displacement of the Pb site away from its mean position towards the displaced *B* site, along either ⟨110⟩ or ⟨100⟩, appears to rotate or distort the unit cell. However, the errors present in the measurements make this observation subject to conjecture. Attempts were made to quantify such a rotation in the unit cell in PMN but the results obtained were ambiguous owing primarily to the difficulty of precisely identifying the centres of the projected atomic columns and partly to the errors inherent in using the various graphics methods.

The area of the sample we observe in HAADF is only a few tens of ånsgröms across – the thickness variation over such a small area is negligible. Each *B*-site column should, theoretically and by definition of the basic structure, contain the species of the *B*-site cations arranged down the column precisely in accordance with the ideal stoichiometry of the compound. The notion that the larger cation species is displaced towards the Pb site by a greater distance than the cation species that have smaller diameters has been proposed by Chen *et al.* (1996). There is no definitive proof for this in the HAADF images, mainly because of the averaging of the intensities along the atomic columns, despite the non-stoichiometry and the fact that there is a size difference between the two *B*-site species. It is plausible that the distribution of the *B*-site cations along the columns is not stoichiometric, resulting in mixed occupancy or random distribution along the columns, and thus leading to differing displacements and ordering arrangements. This could also be a plausible reason for the commonly observed differences in columnar intensities in HAADF. It also appears that the *B*-site positions (ignoring possible non-stoichiometry either on the *B* sites or on the *A* sites) have a profound effect on the behaviour of the Pb ions, at least in PMN, where Pb distortions are more prominent. This highlights the question of whether it is the lone pair on Pb alone or the size and charge difference, as well as non-stoichiometry in the *B*-site cation species, that influence the Pb displacements.

5. Conclusions

The evidence collected from the Cs-corrected HAADF–STEM studies carried out on PMN ceramics and PZN crystals confirms that the *B*-site cations undergo cooperative displacements along ⟨110⟩. The *B*-site cations display correlated planar defect configurations of notable magnitude, especially in PMN. It became evident that the *B*-site cations had undergone substantial displacements, of about 0.50 (20) Å (in PMN) towards the Pb ions. These studies indicate that there are short-range ⟨110⟩ displacements and, to a lesser extent, ⟨100⟩ displacements of the Pb ions on certain sites, at least in PMN. In view of the evidence, it is plausible that the systematic displacements of the *B* sites may be responsible for the continuous streaks, since they represent continuous planar displacements in correlation with Pb ions observed on the {110} planes, as observed in the HAADF patterns. It is also likely that the broadening in the streaks may originate partly from irregularities in Pb ion planar displacements and partly from the observed irregularities in the *B*-site displacements, which might be associated with either random occupancy or ionic size differences between *B′* and *B″* cations.

In the relaxors we have studied, Pb^{2+} and notably *B*-site displacements are present, but the degree of order/disorder in the *B*-site cations dictates how cooperative (in terms of all of the displacements being in the same direction) the displacements are. If the displacements are sufficiently cooperative in the long range, then a phase transition should occur and superstructure spots should ultimately appear in the diffraction patterns instead of streaks, while the dielectric response would entail normal ferroelectric or antiferroelectric states. However, even in the most highly ordered PST samples exhibiting frustrated incommensurate antiferroelectric transitions, it has been impossible to eliminate the continuous diffuse streaking along [110] (Baba-Kishi & Pasciak, 2010), despite the concurrent occurrence of new superstructure reflections along [110]. The simulated displacement value of 0.5 Å for the Pb ions is sufficiently large to be observed in the Cs-corrected STEM images, yet we note that the Pb ions are apparently fixed in their positions relative to the *B* sites as prescribed by the ideal structure. HAADF images from PMN show, however, that some displacement of the Pb ions occurs towards the *B* sites. The observed Pb displacements occur along ⟨110⟩ but appear to occur with short-range order. Assuming the HAADF images from PMN and PZN are representative and correctly interpreted in this article, it appears that the interactions between the various ions in these relaxors are more complex than have so far been envisaged.

The author gratefully acknowledges valuable discussions with Patrick M. Woodward of Ohio State University. Collaboration with Noriaki Endo, Toshihiko Takebe and Tetsuo Oikawa of JEOL Ltd, where the Cs-corrected electron microscopy studies were performed *via* JEOL JEM-ARM200F and JEM 2010FE STEMs, and discussions with Richard Welberry and Marek Pasciak are acknowledged.

References

Baba-Kishi, K. Z., Cressey, G. & Cernik, R. J. (1992). *J. Appl. Cryst.* **25**, 477–487.
Baba-Kishi, K. Z. & Pasciak, M. (2010). *J. Appl. Cryst.* **43**, 140–150.
Baba-Kishi, K. Z., Tai, C. W. & Meng, X. (2006). *Philos. Mag.* **86**, 5031–5051.
Baba-Kishi, K. Z., Welberry, T. R. & Withers, R. L. (2008). *J. Appl. Cryst.* **41**, 930–938.
Chen, I.-W., Li, P. & Wang, Y. (1996). *J. Phys. Chem. Solids*, **57**, 1525–1536.
Davies, P. K. & Akbas, M. A. (2000). *J. Phys. Chem. Solids*, **61**, 159–166.
Dmowski, W., Akbas, M. K., Davies, P. K. & Egami, T. (2000). *J. Phys. Chem. Solids*, **61**, 229–237.
James, E. M. & Browning, N. D. (1999). *Ultramicroscopy*, **78**, 125–139.
Klenov, D. O., Findlay, S. D., Allen, L. J. & Stemmer, S. (2007). *Phys. Rev. B*, **76**, 014111.
Knight, K. S. & Baba-Kishi, K. Z. (1995). *Ferroelectrics*, **173**, 341–349.

Krivanek, O. L., Nellist, P. D., Dellby, N., Murfitt, M. F. & Szilagyi, Z. (2003). *Ultramicroscopy*, **96**, 229–237.
Mihailova, B., Maier, B., Paulmann, C., Malcherek, T., Ihringer, J., Gospodinov, M., Stosch, R., Gutter, B. & Bismayer, U. (2008). *Phys. Rev. B*, **77**, 174106.
Molina, S. I., Varela, M., Sales, D. L., Ben, T., Pizarro, J., Galindo, P. L., Fuster, D., Gonzalez, Y., Gonzalez, L. & Pennycook, S. J. (2007). *Appl. Phys. Lett.* **91**, 143112.
Pasciak, M., Wolcyrz, M. & Pietraszko, A. (2007). *Phys. Rev. B*, **76**, 014117.
Pennycook, S. J. & Jesson, D. E. (1990). *Phys. Rev. Lett.* **64**, 938–941.
Pennycook, S. J. & Jesson, D. E. (1991). *Ultramicroscopy*, **37**, 14–38.
Perrin, C., Menguy, N., Bidault, O., Zahra, C. Y., Zahra, A.-M., Caranoni, C., Hilczer, B. & Stepanov, A. (2001). *J. Phys. Condens. Matter*, **13**, 10231–10245.
Welberry, T. R. & Goossens, D. J. (2008). *J. Appl. Cryst.* **41**, 606–614.
Welberry, T. R., Goossens, D. J. & Gutmann, M. J. (2006). *Phys. Rev. B*, **74**, 224108.
Welberry, T. R., Gutmann, M. J., Woo, H., Goossens, D. J., Xu, G., Stock, C., Chen, W. & Ye, Z.-G. (2005). *J. Appl. Cryst.* **38**, 639–647.
Withers, R. L., Welberry, T. R. & Schmid, S. (1994). *J. Mater. Sci. Forum*, **150–151**, 85–96.
Woodward, P. M. & Baba-Kishi, K. Z. (2002). *J. Appl. Cryst.* **35**, 233–242.
Zhang, L., Dong, M. & Ye, Z.-G. (2000). *Mater. Sci. Eng. B*, **78**, 96–104.